Fusion of radioactive ^{132}Sn with ^{64}Ni at sub-barrier energies

J. F. Liang (梁君健), D. Shapira, C. J. Gross, R. L. Varner, J. R. Beene, P. E. Mueller, and D. W. Stracener
Physics Division, Oak Ridge National Laboratory, Oak Ridge, Tennessee 37831, USA
(Received 25 April 2008; published 7 October 2008)

Sub-barrier fusion of ^{132}Sn and ^{64}Ni was measured at $E_{\rm beam} = 465$ MeV with an improved apparatus. The result of this new measurement is well reproduced by a coupled-channel calculation and a density-constrained time-dependent Hartree-Fock calculation. The previously measured cross section at $E_{\rm beam} = 453$ MeV was reanalyzed. Only an upper limit of the cross section was obtained.

DOI: 10.1103/PhysRevC.78.047601 PACS number(s): 25.60.Pj

The use of neutron-rich radioactive isotope beams for synthesizing heavy elements has been discussed regularly in recent years [1–6]. Due to the excess neutrons in these nuclei, neutron transfer reactions are predicted to enhance fusion rates [4,7]. Many experiments have been performed to study fusion induced by medium-mass neutron-rich radioactive nuclei [8–12]. We have measured the fusion excitation function for ^{132}Sn on ^{64}Ni and observed large sub-barrier fusion enhancement [12]. A coupled-channel calculation including neutron transfer and inelastic excitation of the projectile and target is in good agreement with the measured excitation function except for the lowest energy data point. A density-constrained time-dependent Hartree-Fock (TDHF) calculation [13] also reproduces the measurement fairly well but significantly underpredicts the data point at the lowest energy ($E_{\rm beam} =$ 453 MeV). However, the uncertainty of that data point is fairly large. To investigate the disagreement between the data and the predictions, further measurements were performed. This report presents the result of a new measurement at $E_{\rm beam} = 465$ MeV using an improved apparatus to provide further information on the cross section at low energy and to provide an indirect test of the the lowest energy data point in the previous experiment.

The measurements were carried out at the Holifield Radioactive Ion Beam Facility at Oak Ridge National Laboratory. The ^{132}Sn beam was produced from the fission of ^{238}U nuclei using the Isotope Separator On-Line technique. The ^{132}Sn beam, postaccelerated by the 25 MV tandem electrostatic accelerator, was incident on a 1 mg/cm^2 ^{64}Ni target. Reaction products were detected in a multianode ionization chamber positioned 18.2 cm downstream of the target. A position sensitive timing detector was placed in front of the ionization chamber to measure time-of-flight and to monitor the position of the beam on the target. The ionization chamber had three anodes. The gas pressure in the ionization chamber, 40 Torr of CF_4, was adjusted such that the evaporation residues (ERs) lost more than 75% of their energy in the first two sections. The beam and beam-like particle events in which the energy deposited in the third section was too high were vetoed. This reduced the background for measurements of small cross sections. To verify that the improved apparatus worked correctly, the data point at $E_{\rm c.m.} = 151$ MeV ($E_{\rm beam} =$ 475 MeV) was remeasured. Because the fission decay of the compound nucleus is negligible at sub-barrier energies [12], only the ER cross section was measured. The ERs were identified by measuring the energy loss in the ionization chamber and the time-of-flight with microchannel plate timing detectors. A detailed description of the apparatus and the method used in data reduction and analysis is given in Refs. [12] and [14].

The time-of-flight spectrum was divided into bins 0.66 ns wide to search for ERs. Figure 1 displays a histogram for the energy loss in the first two sections of the ionization chamber in the timing bin centered at 4 ns later than the beam arrival time. This time-of-flight is where the ERs are expected. A group of ERs can be identified clearly. The time distribution of ERs is shown in Fig. 2. Zero time corresponds to the beam arrival time. The rate for beam-like particles was suppressed by a time cutoff applied via a timing pretrigger [14]. The total number of ERs was obtained by summing over the number of counts in the peak region between 3 and 5 ns. The measured ER cross section, after the correction for detection efficiency [12], was 5 ± 1 mb, which agrees with our previous measurement at $E_{\rm beam} = 475$ MeV.

Instead of making a measurement at the previous lowest energy point ($E_{\rm beam} = 453$ MeV), a 465 MeV beam, close to halfway between 453 and 475 MeV, was chosen. A histogram of the energy loss in the first two sections of the ionization chamber in the timing bin centered at 4 ns later than the beam arrival time is shown in Fig. 3. More background is visible here than at 475 MeV because the ER cross section is smaller and therefore required a longer measurement time. To determine where the ERs should appear, the energy loss for the beam and ERs in the ionization chamber was estimated [15]. Because the change in energy loss between the 475 and 465 MeV measurements was small, the location of the ERs in the energy loss histogram for the 465 MeV measurement can be estimated accurately using the energy calibration of the energy loss spectra and the 475 MeV measurement. The gate in the histogram in Fig. 3 was drawn according to this estimate. A time distribution of the ERs is shown in Fig. 4. It can be seen that there is a prominent peak near 4 ns which is where the ERs are expected. The total number of ERs was obtained by summing over the number of counts in the peak region between 3 and 5 ns and subtracting the background obtained by fitting a linear function to it as shown by the dashed curve. The measured ER cross section, after the correction for detection efficiency, was 0.7 ± 0.2 mb. The effective reaction energy deduced from the thick target yield method [12] was $148 \pm$ 2 MeV. In Fig. 4, the background increases substantially for the time-of-flight closer to the beam. It is exhibited in the increase

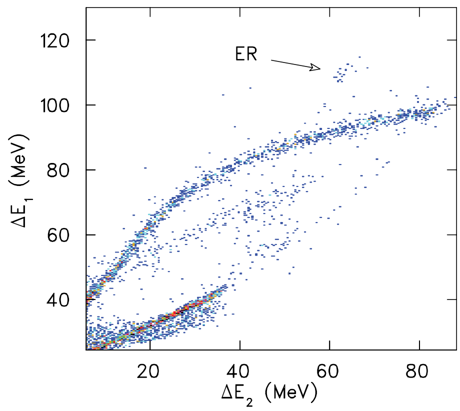

FIG. 1. (Color online) Two-dimensional histogram of energy loss of particles in the first two sections of the ionization chamber. The ERs produced in 475 MeV ^{132}Sn on ^{64}Ni are well separated from the scattered beams and labeled above.

in the number of counts near 2 ns. The yield for beam-like particles was suppressed in the 1 ns region because of the time cutoff applied via a timing pretrigger.

The fusion excitation function including the data point measured in this work is shown in Fig. 5. A coupled-channel calculation taking into account neutron transfer and inelastic excitation of the projectile and target and a density-constrained TDHF calculation reproduce the new measurement very well.

Although the beam energy for the data point in question in our previous measurement was 12 MeV lower, the magnitude of the cross section was reported to be comparable to the present 465 MeV. Extrapolations from the present measurement by theoretical predictions suggest that the cross section at $E_{\mathrm{beam}} = 453$ MeV is more than an order of magnitude smaller than the newly measured cross section at $E_{\mathrm{beam}} = 465$ MeV. We have reanalyzed all the data from the previous experiment. In that experiment, the timing pretrigger was not optimized for some beam energies. Figure 6(a) displays the time-of-flight spectrum for $E_{\mathrm{beam}} = 465$ MeV measured in the present work with the timing pretrigger applied. The narrow peak on the left-hand side is the result of the beam yield scaled down by a factor of 1000. As mentioned above, the peak of the beam time-of-flight was taken as zero time. Therefore, ERs

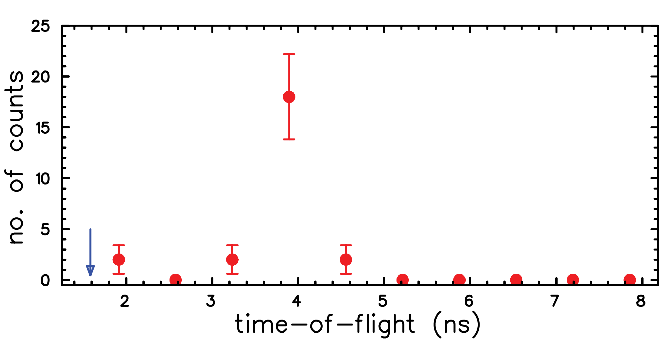

FIG. 2. (Color online) Time distribution of ERs produced in 475 MeV ^{132}Sn on ^{64}Ni. The time cutoff for the timing pretrigger is shown by the downward arrow. The data shown are a partial sample of the entire data set.

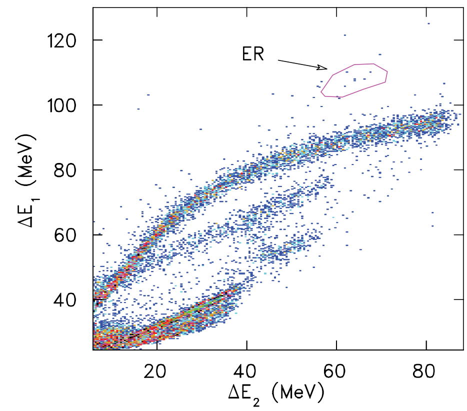

FIG. 3. (Color online) Two-dimensional histogram of energy loss of particles in the first two sections of the ionization chamber. The ERs produced in 465 MeV ^{132}Sn on ^{64}Ni are located in the gate.

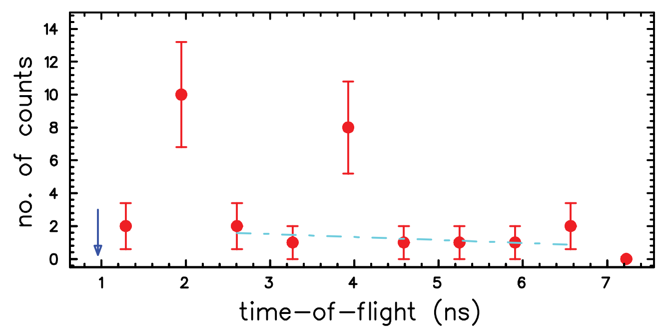

FIG. 4. (Color online) Time distribution of ERs produced in 465 MeV ^{132}Sn on ^{64}Ni. The dashed curve is the result of fitting the background by a linear function. The time cutoff for the timing pretrigger is shown by the downward arrow. The data shown are a partial sample of the entire data set.

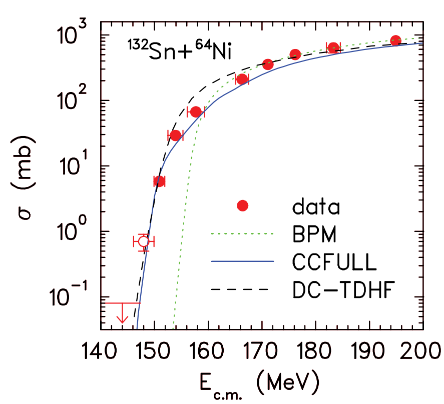

FIG. 5. (Color online) Fusion excitation function of ^{132}Sn on ^{64}Ni. The data point measured in this work is shown by the open circle. The downward arrow represents the upper limit of the cross section obtained by the reanalysis of the lowest energy data point in our previous measurement. The horizontal bar displays the spread of the beam energy in the target. The prediction of a one-dimensional barrier penetration model is shown by the dotted curve, the coupled-channel calculation including neutron transfer and inelastic excitation of the projectile and target is shown by the solid curve, and the density-constrained TDHF calculation is shown by the dashed curve.

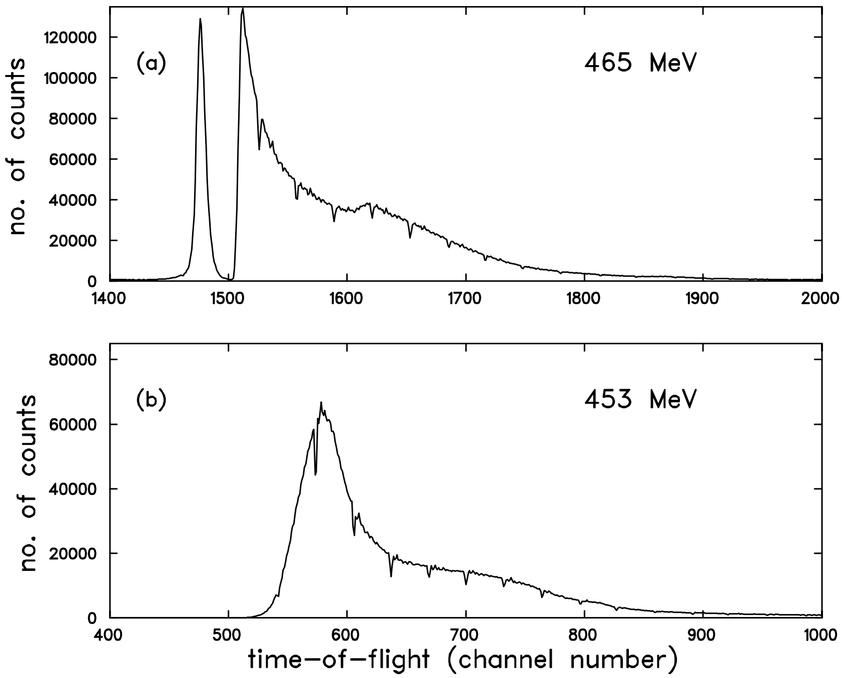

FIG. 6. (a) Time-of-flight spectrum for 465 MeV $^{132}Sn + ^{64}Ni$ from this work. The peak on the left-hand side corresponds to the yield of the beam scaled down by a factor of 1000. The calibration for the time-of-flight is 33 ps per channel. (b) Time-of-flight spectrum for 453 MeV $^{132}Sn + ^{64}Ni$ from our previous measurement.

were expected 4 ns after the beam arrival time and located to the right side of the peak. The time-of-flight spectrum for the previous measurement at $E_{beam} = 453$ MeV is shown in Fig. 6(b). The peak corresponding to the beam was not clearly seen. As such, the time zero was taken from the left leading edge of the spectrum. Because the centroid and the width of the peak for the beam could not be determined, it resulted in uncertainties for locating the time window in which ERs were expected. The results of the reanalysis of the previous measurements agree with the published results [12] except at the lowest energy ($E_{beam} = 453$ MeV) where an upper limit of the cross section was obtained to be 0.08 mb. This value is comparable to the sensitivity limit for our apparatus based on an analysis of the background. This should be sufficient for most of the sub-barrier fusion studies. If one wants to pursue measurements for cross sections significantly less than 1 mb, large acceptance gas-filled separators that can effectively suppress beam-like particles at the focal plane would be more suitable.

Research at the Oak Ridge National Laboratory is supported by the U.S. Department of Energy under Contract DE-AC05-00OR22725 with UT-Battelle, LLC.

[1] G. Münzenberg, Philos. Trans. R. Soc. London A **356**, 2083 (1998).
[2] G. G. Adamian, N. V. Antonenko, and W. Scheid, Nucl. Phys. **A678**, 24 (2000).
[3] G. G. Adamian, N. V. Antonenko, and W. Scheid, Phys. Rev. C **69**, 044601 (2004).
[4] V. I. Zagrebaev, Prog. Theor. Phys. Suppl. **154**, 122 (2004).
[5] Y. Aritomo, Phys. Rev. C **75**, 024602 (2007).
[6] W. Loveland, Phys. Rev. C **76**, 014612 (2007).
[7] V. Yu. Denisov, Eur. Phys. J. A **7**, 87 (2000).
[8] K. E. Zyromski *et al.*, Phys. Rev. C **63**, 024615 (2001).
[9] Y. X. Watanabe *et al.*, Eur. Phys. J. A **10**, 273 (2001).
[10] J. F. Liang and C. Signorini, Int. J. Mod. Phys. E **14**, 1121 (2005).
[11] W. Loveland, D. Peterson, A. M. Vinodkumar, P. H. Sprunger, D. Shapira, J. F. Liang, G. A. Souliotis, D. J. Morrissey, and P. Lofy, Phys. Rev. C **74**, 044607 (2006).
[12] J. F. Liang *et al.*, Phys. Rev. C **75**, 054607 (2007).
[13] A. S. Umar and V. E. Oberacker, Phys. Rev. C **76**, 014614 (2007).
[14] D. Shapira *et al.*, Nucl. Instrum. Methods Phys. Res. A **551**, 330 (2005).
[15] J. F. Ziegler, *Handbook of Stopping Cross Sections for Energetic Ions in All Elements* (Pergamon Press, New York, 1980).